

See discussions, stats, and author profiles for this publication at: <https://www.researchgate.net/publication/231654126>

Efficient Photocatalytic Removal of Contaminant by Bi₃NbxTa_{1-x}O₇ Nanoparticles Under Visible Light Irradiation

ARTICLE in THE JOURNAL OF PHYSICAL CHEMISTRY C · NOVEMBER 2009

Impact Factor: 4.77 · DOI: 10.1021/jp907831y

CITATIONS

31

READS

26

5 AUTHORS, INCLUDING:



Gaoke Zhang

Wuhan University of Technology

182 PUBLICATIONS 2,245 CITATIONS

[SEE PROFILE](#)



Shujie Yu

North China Electric Power University

7 PUBLICATIONS 171 CITATIONS

[SEE PROFILE](#)

Efficient Photocatalytic Removal of Contaminant by $\text{Bi}_3\text{Nb}_x\text{Ta}_{1-x}\text{O}_7$ Nanoparticles under Visible Light Irradiation

Shuiming Zhang,[†] Gaoke Zhang,^{*,†} Shujie Yu,[†] Xiaoguo Chen,[†] and Xiaoyang Zhang[‡]

School of Resources and Environmental Engineering, Wuhan University of Technology, 122 Luoshi Road, Wuhan 430070, P. R. China, and State Key Laboratory of Crystal Materials, Shandong University, 27 Shanda Nanlu, Jinan 250100, P. R. China

Received: August 13, 2009; Revised Manuscript Received: September 26, 2009

Nanosized $\text{Bi}_3\text{Nb}_x\text{Ta}_{1-x}\text{O}_7$ photocatalysts were prepared by a facile and low-cost sol–gel method using stable, less toxic Ta_2O_5 , Nb_2O_5 , and $\text{Bi}(\text{NO}_3)_3 \cdot 5\text{H}_2\text{O}$ as the raw materials. The as-prepared samples were characterized by X-ray diffraction, transmission electron microscopy, Fourier transformation infrared spectroscopy, X-ray photoelectron spectroscopy, and UV–vis diffuse reflectance spectroscopy. The $\text{Bi}_3\text{Nb}_x\text{Ta}_{1-x}\text{O}_7$ nanoparticles exhibited an efficient photocatalytic activity in the decomposition of acid red G (ARG) dye solution under visible light irradiation. Besides decoloring, the typical sample $\text{Bi}_3\text{Nb}_{0.6}\text{Ta}_{0.4}\text{O}_7$ also showed an excellent photocatalytic property for the removal of the cyanotoxin, microcystin-LR (MC-LR, an emerging contaminant from the Contaminant Candidate Lists (CCLs 1–3) of the USEPA). The excellent visible light photocatalytic activity of the samples was mainly attributed to their narrow band gaps, small particle size, and the oxygen vacancies on the surface of the catalysts. According to experimental results, a possible mechanism of the photocatalysis over $\text{Bi}_3\text{Nb}_x\text{Ta}_{1-x}\text{O}_7$ was proposed.

1. Introduction

Recently, semiconductor photocatalysts have attracted extensive attention because of their wide applications in solar energy conversion and environmental purification.^{1–4} To date, the remarkable progress of photocatalysis has been mainly focused on TiO_2 -based materials due to their high photocatalytic activity and stability.^{5–8} However, TiO_2 is only active in the ultraviolet (UV) light range, which accounts for a small fraction in solar light. From a viewpoint of the efficient utilization of solar light, a lot of work has been done to develop visible-light-driven photocatalysts. One of the efforts in the development is modification of TiO_2 by doping or ion-implanting methods.^{9–13} However, doped materials often suffer from thermal instability,⁹ and the doping process may require expensive ion implantation equipment.¹⁴ Another approach to realize visible light photocatalysis is to develop new photocatalytic materials independent of TiO_2 .^{15–19} In recent years, a family of Bi-based oxides has been found to be very active under visible light irradiation, which is attributed to the hybridized valence band by O 2p and Bi 6s so as to narrow the band gap.^{20–23}

Many of niobates and tantalates have also been attracted great attention because of their high photocatalytic properties.^{24–27} However, most of these photocatalysts are mainly synthesized by the solid-state (SS) method at high temperature and only have photocatalytic activity under the UV light region. The photocatalyst obtained by the SS method often has small specific surface area, large particle size, and low adsorbability, which result in low photocatalytic efficiency in the treatment of pollutants at very low concentration in the environment. In contrast, wet chemical routes are a promising alternative, since they can well control the whole process from the molecular

precursor to the final material to give highly pure and homogeneous materials. In addition, wet routes allow low reaction temperature, so that the size of the synthesized particles may be well controlled.^{28,29} Several synthesis routes have been developed to prepare the nanosized tantalum- or niobium-based compounds. However, most of these methods use niobium or tantalum alkoxides as the sources, which have many serious drawbacks, such as inflammability, relatively high cost, and great sensitivity to moisture. All of these undesirable characteristics limit its general application.³⁰ Therefore, it is important to develop nanosized niobates and tantalates photocatalysts which have high photocatalytic activity in visible light region via a facile and low-cost sol–gel method at lower temperature.

In the present paper, we used Ta_2O_5 , Nb_2O_5 , and $\text{Bi}(\text{NO}_3)_3 \cdot 5\text{H}_2\text{O}$ as the raw materials and successfully synthesized $\text{Bi}_3\text{Nb}_x\text{Ta}_{1-x}\text{O}_7$ ($x = 0–1$) solid solution photocatalysts through a facile sol–gel method at lower temperature by changing the initial concentration of the reactants. The photocatalytic properties were evaluated by the degradation of acid red G (ARG) and microcystin-LR (MC-LR) under visible light irradiation. It was demonstrated that the as-obtained samples exhibited an excellent visible light photocatalytic acitivity for the degradation of the pollutants.

2. Experimental Section

2.1. Preparation. Ta_2O_5 , Nb_2O_5 , bismuth nitrate pentahydrate ($\text{Bi}(\text{NO}_3)_3 \cdot 5\text{H}_2\text{O}$), potassium hydroxide (KOH), citric acid (CA), nitric acid (HNO_3), oxalic acid (OA), ammonia ($\text{NH}_3 \cdot \text{H}_2\text{O}$), and ethylenediaminetetraacetic acid (EDTA) were used as starting chemical reagents. All of the reagents were analytical grade and were used without further purification.

The $\text{Bi}_3\text{Nb}_x\text{Ta}_{1-x}\text{O}_7$ samples were prepared by a sol–gel method. First, Ta_2O_5 was mixed with KOH according to a molar ratio of 1:10 and was then sintered at 500 °C. The sintered substances were leached with hot deionized water, and after filtration, a transparent solution was obtained. The tantalum acid

* Corresponding author: Tel 86-27-87651816; fax 86-27-87887445; e-mail gkzhang@whut.edu.cn.

† Wuhan University of Technology.

‡ Shandong University.

sediment was obtained after adjusting the pH of the solution to 1–2 using nitric acid and was then washed successively until the potassium ions were completely removed. The as-prepared tantalic acid was dissolved in oxalic acid solution, and a tantalum–oxalic acid solution (Ta–OA) was obtained. The niobium–oxalic acid solution (Nb–OA) was prepared by the hydrothermal method reported in our previous study.³¹ The concentrations of tantalum and niobium in their solution were determined by inductively coupled plasma–atomic emission spectrometry (ICP-AES). Second, $\text{Bi}(\text{NO}_3)_3 \cdot 5\text{H}_2\text{O}$ was added into citric acid solution, and then EDTA–ammonia solution was added slowly into the solution under continuous stirring until $\text{Bi}(\text{NO}_3)_3 \cdot 5\text{H}_2\text{O}$ was absolutely dissolved and the Bi–CA solution was obtained.

Third, Ta–OA, Nb–OA, and Bi–CA solutions were mixed together according to the composition $\text{Bi}_3\text{Nb}_x\text{Ta}_{1-x}\text{O}_7$ ($x = 0, 0.2, 0.4, 0.6, 0.8$, and 1.0). The as-obtained solution was stirred at 80°C until it became transparent colloidal and was then heated until the formation of dark-colored, amorphous polymeric precursors occurred. The precursors were subjected to calcination at 300°C to remove the organics and then were ground and sintered at 450°C for 4 h. Finally, the $\text{Bi}_3\text{Nb}_x\text{Ta}_{1-x}\text{O}_7$ nanoparticles were obtained.

2.2. Characterization. The structure and crystallinity of the as-prepared samples were characterized by powder X-ray diffraction (XRD) on a D/MAX-RB powder X-ray diffractometer (Rigaku, Japan) using $\text{Cu K}\alpha$ radiation under the operation conditions of 40 kV and 50 mA . The morphology and microstructure of the as-obtained samples were analyzed by transmission electron microscopy (TEM) and high-resolution transmission electron microscopy (HRTEM) with a JEM-2100F electron microscope (JEOL, Japan), using a 200 kV accelerating voltage. The absorption edge of the $\text{Bi}_3\text{Nb}_x\text{Ta}_{1-x}\text{O}_7$ samples was measured by a UV–vis spectrophotometer (UV2550, Shimadzu, Japan). The chemical bonds on the surface of the catalysts were detected by the Fourier transform infrared spectroscopy (FT-IR) (Nexus, Thermo Nicolet). X-ray photoelectron spectroscopy (XPS) analysis was carried out by using a Thermo VG Multilab 2000 spectrometer (UK) with a monochromatic $\text{Al K}\alpha$ source and a charge neutralizer. All binding energies were referred to the C 1s peak at 284.63 eV of the surface adventitious carbon and revised. The generation of $\cdot\text{OH}$ radicals was investigated by the photoluminescence (PL) technique with terephthalic acid (TA).³² The $\cdot\text{OH}$ trapping fluorescence spectra was measured with a fluorescence spectrophotometer (RF-5300PC, Shimadzu, Japan).

2.3. Photocatalytic Activity Measurement. The photocatalytic activities of the $\text{Bi}_3\text{Nb}_x\text{Ta}_{1-x}\text{O}_7$ samples were evaluated by the degradation of ARG and MC-LR under visible light irradiation. For the photocatalytic degradation of ARG, 0.15 g of the as-prepared catalyst was added into 100 mL of ARG aqueous solution (50 mg/L , $\text{pH} = 6.8$). Before illumination, the mixture was stirred for 5 min in darkness to disperse the catalyst. The reactor was then irradiated with visible light emitted by a 300 W Dy lamp with a 400 nm cutoff filter. The concentration of ARG aqueous solution was analyzed using a UV–vis spectrophotometer (UV751GD, China) at its maximum absorption wavelength of 505 nm .

For the degradation of MC-LR, which was purified from a laboratory culture of *Microcystis aeruginosa*, 0.05 g of the as-prepared $\text{Bi}_3\text{Nb}_{0.6}\text{Ta}_{0.4}\text{O}_7$ photocatalyst was suspended in 20 mL of MC-LR solution ($\text{pH} = 5.9 \pm 0.1$ with super quality water) with the initial concentration of 3.1 mg/L in a glass reactor. The reaction temperature was kept at room temperature using

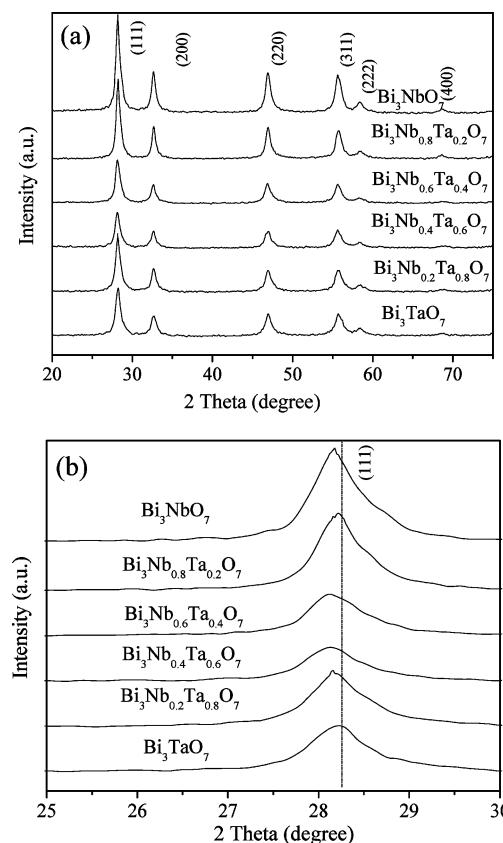


Figure 1. (a) XRD patterns of $\text{Bi}_3\text{Nb}_x\text{Ta}_{1-x}\text{O}_7$ prepared at 450°C for 4 h. (b) Enlarged part of the $\text{Bi}_3\text{Nb}_x\text{Ta}_{1-x}\text{O}_7$ XRD patterns ranging from $2\theta = 25^\circ\text{--}30^\circ$.

a water cooling device. Before illumination, the suspension was stirred for 30 min in darkness to disperse the catalyst. The reactor was then irradiated with visible light emitted by a 300 W Dy lamp with a 400 nm cutoff filter. A sample of 1 mL was taken and centrifuged to remove the photocatalyst particles. The samples were equally split in 0.2 mL inserts placed in vials and analyzed with high-performance liquid chromatography (HPLC, Agilent Series 1100) for the quantification of MC-LR. For the HPLC analysis, the injection volume to a C-18 Discovery column (Supelco) at 40°C was $10\text{ }\mu\text{L}$. The mobile phase in isocratic mode with a flow rate of 1 mL/min was a mixture of methanol and 0.01% trifluoroacetic acid (TFA) in water at a ratio of $60:40$. MC-LR was measured with a photodiode array detector at 238 nm .

3. Results and Discussion

3.1. Characterization. Figure 1 shows the XRD patterns of the $\text{Bi}_3\text{Nb}_x\text{Ta}_{1-x}\text{O}_7$ solid solutions prepared by the sol–gel method at 450°C for 4 h. It is important to note that no reflections from Nb_2O_5 , Ta_2O_5 , or other species were observed as distinct impurities. The patterns of Bi_3TaO_7 and Bi_3NbO_7 could be readily indexed to JCPDS (44-0202) and JCPDS (86-0875), respectively. Despite the different composition, the similarity of the diffractograms suggests that the compounds $\text{Bi}_3\text{Nb}_x\text{Ta}_{1-x}\text{O}_7$ ($x = 0, 0.2, 0.4, 0.6$, and 0.8) are isostructural with Bi_3NbO_7 . Figure 1b shows that the (111) peak slightly shifted to smaller angles with the increase in x . The broad diffraction peaks of the $\text{Bi}_3\text{Nb}_x\text{Ta}_{1-x}\text{O}_7$ solid solutions imply the small crystal size of the products. The peak at 28.2° was used for the calculation of the crystal size because it had a relatively strong intensity and did not overlap with the other

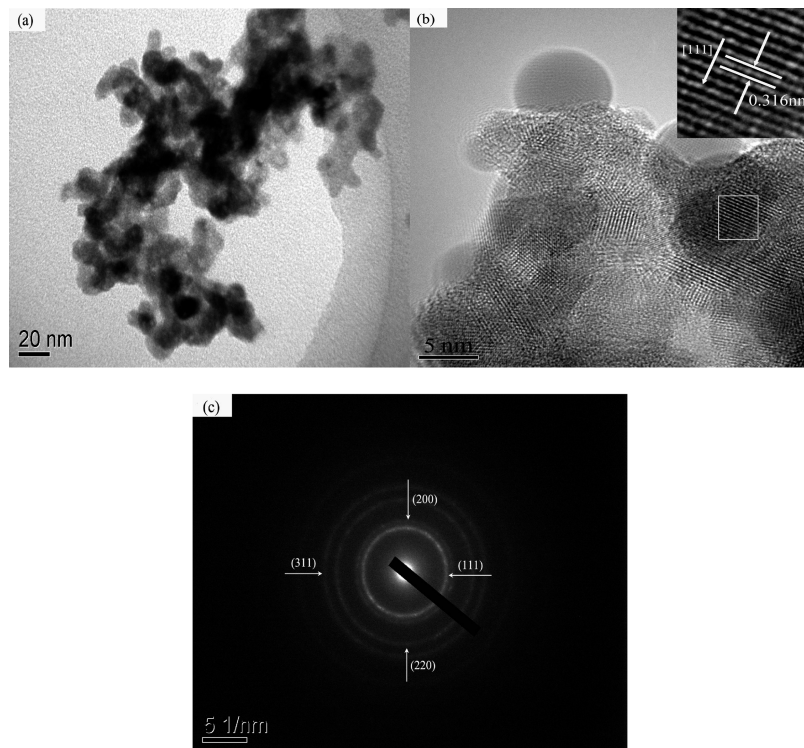


Figure 2. TEM images of $\text{Bi}_3\text{Nb}_{0.6}\text{Ta}_{0.4}\text{O}_7$ nanoparticles: (a) TEM image; (b) HRTEM image; (c) SAED pattern.

diffraction peaks. The average crystal size of the as-prepared samples was about 15 nm, as estimated by the Scherrer equation.

Figure 2 shows the morphology and microstructure of the typical sample $\text{Bi}_3\text{Nb}_{0.6}\text{Ta}_{0.4}\text{O}_7$. On the basis of TEM observations in Figure 2a, the particle size of the $\text{Bi}_3\text{Nb}_{0.6}\text{Ta}_{0.4}\text{O}_7$ sample is only about 12–15 nm, which agrees well with the value estimated from the XRD pattern. The HRTEM image (Figure 2b) shows the lattice fringes with an interplanar spacing of 0.316 nm corresponds to the (111) plane of the $\text{Bi}_3\text{Nb}_{0.6}\text{Ta}_{0.4}\text{O}_7$ crystal. The selective area electron diffraction (SAED) pattern in Figure 2c can be indexed to (311), (220), (200), and (111) planes, which indicates the particles in Figure 2a were formed by aggregating some nanosized single crystals.

To investigate the chemical state and the surface compositions, XPS studies have been carried out. The XPS result shows the existence of Bi 4f, Nb 3d, and Ta 4f peaks in the $\text{Bi}_3\text{Nb}_{0.6}\text{Ta}_{0.4}\text{O}_7$ sample (see Figure 3). From Figure 3a, the Bi 4f region can be fitted into four peaks 157.6, 159.6, 163.1, and 164.9 eV. The binding energy value of Bi^{3+} state in some Bi-containing compounds is about in the range of 158.2–159.6 eV for Bi 4f_{7/2},^{33,34} which is very close to Bi^{2+} state. In the structure of the compound $\text{Bi}_3\text{Nb}_{0.6}\text{Ta}_{0.4}\text{O}_7$, there exist two different Bi–O distances, ranging from 1.94 to 2.61 Å.^{35,36} The two strong peaks taken for the Bi region at 164.9 and 159.6 eV are assigned to the Bi 4f_{5/2} and Bi 4f_{7/2} peaks of $\text{Bi}^{3+}(1)$ in the short Bi–O bonds. The lower binding energy peaks (163.1, 157.6 eV) correspond to the Bi 4f_{5/2} and Bi 4f_{7/2} peaks of the $\text{Bi}^{3+}(2)$ in the long Bi–O bonds. The lower binding energy peaks (163.1, 157.6 eV) also indicated the possibility appearance of Bi^{3-x} at the surface of $\text{Bi}_3\text{Nb}_{0.6}\text{Ta}_{0.4}\text{O}_7$ nanoparticles, which may be due to a deficiency in oxygen and an enhanced concentration of oxygen vacancies in the vicinity of bismuth cations,³⁷ resulting in the higher quantum efficiency of photocatalysis. The peaks with binding energy of 207.9 and 209.8 eV, as displayed in Figure 3b, are for the Nb 3d_{5/2} and Nb 3d_{3/2} region, respectively, which indicates that niobium in the as-

prepared sample exists in Nb⁵⁺.^{22,38} The binding energy at 30.1 and 27.2 eV for Ta 4f_{5/2} and Ta 4f_{7/2} (Figure 3c) can be assigned to the Ta⁵⁺ state.³⁹

UV-vis diffuse reflectance spectra of the $\text{Bi}_3\text{Nb}_x\text{Ta}_{1-x}\text{O}_7$ photocatalysts prepared by the sol–gel method are shown in Figure 4. All the samples have photoabsorption from UV light to visible light, and the wavelengths of the absorption edges are around 443 nm. For a crystalline semiconductor, the optical band gap is determined by the following equation using the optical absorption data near the band edge^{40,41}

$$ahv = A(hv - E_g)^{n/2}$$

where a , v , A , and E_g are the absorption coefficient, light frequency, proportionality constant, and band gap, respectively. In the equation, n decides the characteristics of the transition in a semiconductor, that is, direct transition ($n = 1$) or indirect transition ($n = 4$). The values of n and E_g were determined by the following steps: (1) plot $\ln(ahv)$ vs $\ln(hv - E_g)$, using an approximate value of E_g , and then determine the value of n with the slope of the straightest line near the band edge; (2) plot $(ahv)^{2/n}$ vs hv and then evaluate the band gap E_g by extrapolating the straightest line to the hv axis intercept. Following this method, the value of n for $\text{Bi}_3\text{Nb}_x\text{Ta}_{1-x}\text{O}_7$ was estimated to be 2. This means that the optical transitions for the present compounds are indirectly allowed. The values of the band gaps for the catalysts were estimated to be around 2.80 eV. With an increasing amount of Ta substitution, the absorbance onset of the as-obtained samples showed a slight shift to shorter wavelengths. The results indicate that the $\text{Bi}_3\text{Nb}_x\text{Ta}_{1-x}\text{O}_7$ nanoparticles have a suitable band gap for photocatalytic decomposition of organic contaminants under visible light irradiation.

3.2. Photocatalytic Properties. The photocatalytic activities of the $\text{Bi}_3\text{Nb}_x\text{Ta}_{1-x}\text{O}_7$ samples were evaluated via the degrada-

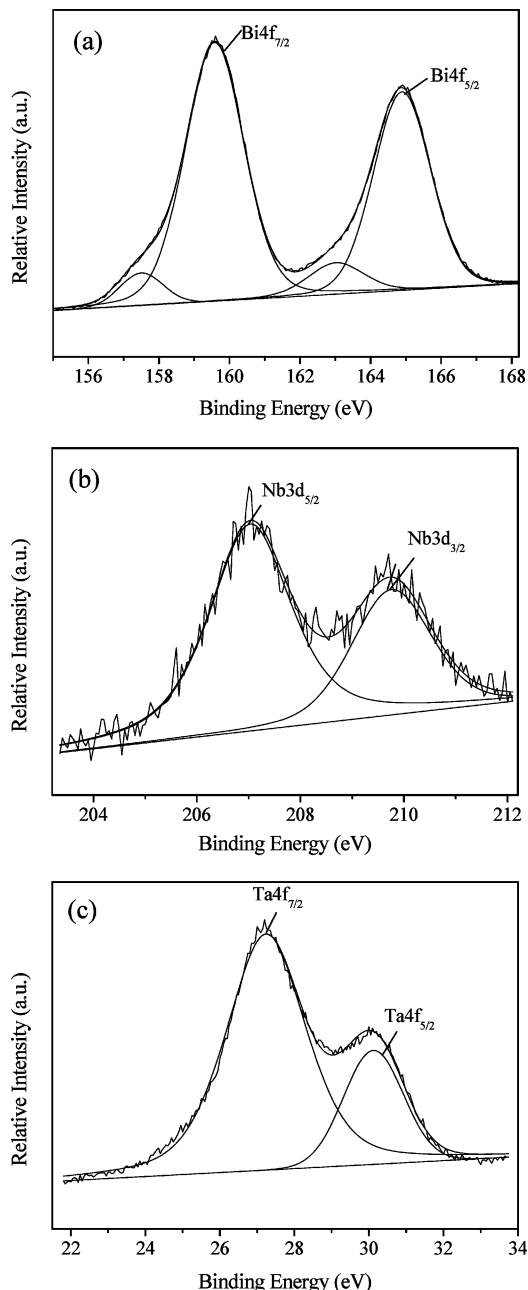


Figure 3. High-resolution XPS spectra of $\text{Bi}_3\text{Nb}_{0.6}\text{Ta}_{0.4}\text{O}_7$ nanopartiles: (a) Bi 4f; (b) Nb 3d; (c) Ta 4f.

tion of ARG and MC-LR under visible light irradiation. Figure 5 displays the photodegradation of ARG over the $\text{Bi}_3\text{Nb}_x\text{Ta}_{1-x}\text{O}_7$ samples under different conditions. As shown in Figure 5a, a blank experiment in the absence of the photocatalyst but under visible light irradiation showed that the photolysis of ARG was negligible. However, with $\text{Bi}_3\text{Nb}_{0.6}\text{Ta}_{0.4}\text{O}_7$ as the photocatalyst, 97% of ARG is decolorized after 120 min, showing the excellent photocatalytic activity of $\text{Bi}_3\text{Nb}_{0.6}\text{Ta}_{0.4}\text{O}_7$ under visible light irradiation. The adsorption of ARG on the $\text{Bi}_3\text{Nb}_{0.6}\text{Ta}_{0.4}\text{O}_7$ sample in the dark was also checked; the concentration of ARG was only decreased 23% after 120 min, suggesting that the decolorizing of ARG is mainly caused by photodegradation but not adsorption. For comparison, the photocatalytic properties of P25 and SS- $\text{Bi}_3\text{Nb}_{0.6}\text{Ta}_{0.4}\text{O}_7$ were also evaluated. After irradiation by visible light for 120 min, the degradation rate of ARG by P25 was only 30%. The pure $\text{Bi}_3\text{Nb}_{0.6}\text{Ta}_{0.4}\text{O}_7$ compound was prepared by a conventional solid-state method at

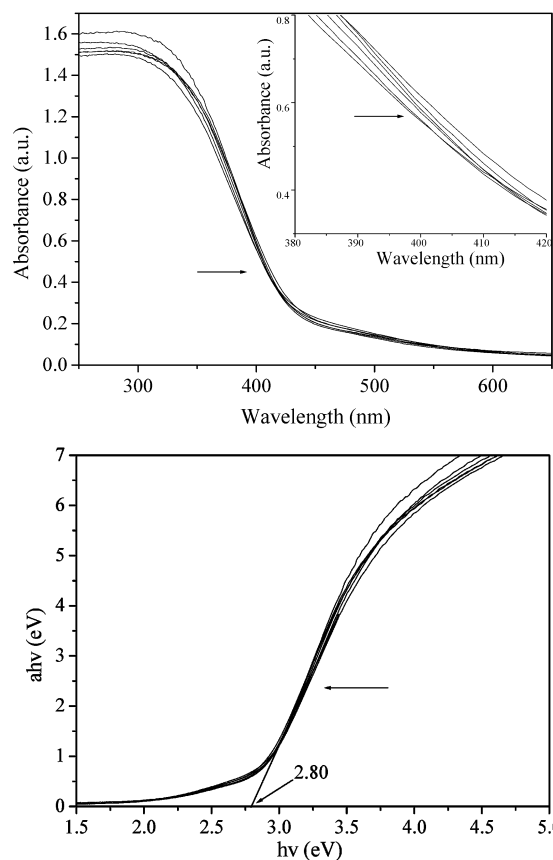


Figure 4. UV-vis diffuse reflectance spectra of the as-prepared $\text{Bi}_3\text{Nb}_x\text{Ta}_{1-x}\text{O}_7$ samples. Arrow direction: $x = 0, 0.2, 0.4, 0.6, 0.8$, and 1.0 .

700 °C for 4 h (SS- $\text{Bi}_3\text{Nb}_{0.6}\text{Ta}_{0.4}\text{O}_7$).⁴² It was found that $\text{Bi}_3\text{Nb}_{0.6}\text{Ta}_{0.4}\text{O}_7$ prepared by the sol-gel method was about 6 times faster than SS- $\text{Bi}_3\text{Nb}_{0.6}\text{Ta}_{0.4}\text{O}_7$ for the decomposition of ARG. This may be attributed to the large particle size of SS- $\text{Bi}_3\text{Nb}_{0.6}\text{Ta}_{0.4}\text{O}_7$, which results in a poor dispersion of catalyst in the solution. As can be seen in Figure 5b, all of the $\text{Bi}_3\text{Nb}_x\text{Ta}_{1-x}\text{O}_7$ samples show the excellent photocatalytic activity under visible light irradiation. With the increase of x , the activity of the as-obtained catalysts slightly increased. Among the $\text{Bi}_3\text{Nb}_x\text{Ta}_{1-x}\text{O}_7$ photocatalysts, $\text{Bi}_3\text{Nb}_{0.6}\text{Ta}_{0.4}\text{O}_7$ shows the highest activity.

Figure 6 displays the temporal evolution of the spectral changes during the photodegradation of ARG over the $\text{Bi}_3\text{Nb}_{0.6}\text{Ta}_{0.4}\text{O}_7$ sample. The absorption spectrum of the original solution shows three distinctive peaks at 215, 330, and 505 nm, which correspond to the structure of the benzene ring, the naphthalene ring, and the nitrogen to nitrogen double bond ($-\text{N}=\text{N}-$), respectively. The decrease of absorption peaks of acid red G at 505 nm means that the nitrogen to nitrogen double bond was destroyed. The specific peaks of the benzene ring and naphthalene ring at 215 and 330 nm become smoother gradually during the degradation processes, which indicated that the catalyst not only destroyed the chromophore of ARG but also decomposed the benzene ring and naphthalene ring partly.²⁶

Figure 7 shows the FT-IR spectra of the $\text{Bi}_3\text{Nb}_{0.6}\text{Ta}_{0.4}\text{O}_7$ nanopowders before and after the photocatalytic reaction of ARG dye. The broad bands between 450 and 1000 cm⁻¹ in two spectra are mainly assignable to $\text{Bi}-\text{O}$, $\text{M}-\text{O}$ ($\text{M} = \text{Nb}$ or Ta), and $\text{M}-\text{O}-\text{M}$ stretching vibrations.⁴³⁻⁴⁵ The bands at about 3430 and 1635 cm⁻¹ can be ascribed to water molecules adsorbed on the surface of the catalysts. The band at 1385–1390

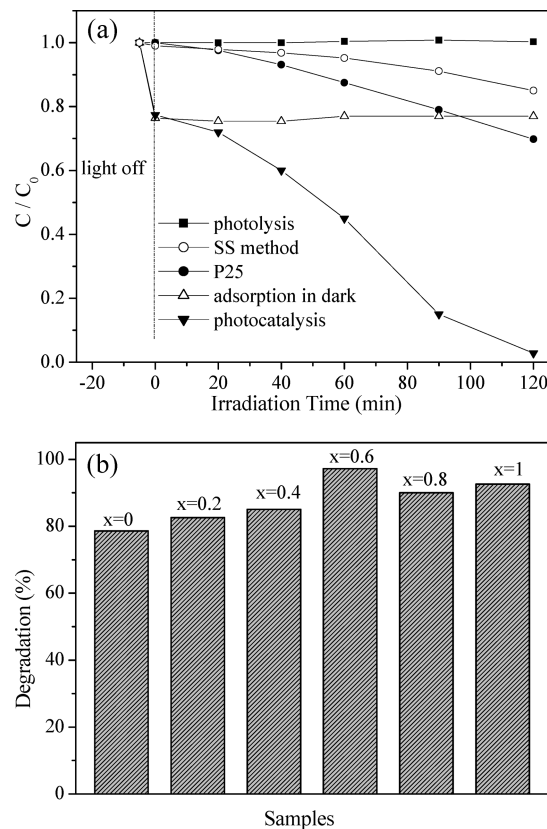


Figure 5. (a) Photocatalytic degradation of ARG solution (50 mg/L) of $\text{Bi}_3\text{Nb}_{0.6}\text{Ta}_{0.4}\text{O}_7$ under different conditions. (b) Photocatalytic degradation of ARG solution over $\text{Bi}_3\text{Nb}_x\text{Ta}_{1-x}\text{O}_7$ nanoparticles under visible light illumination within 120 min.

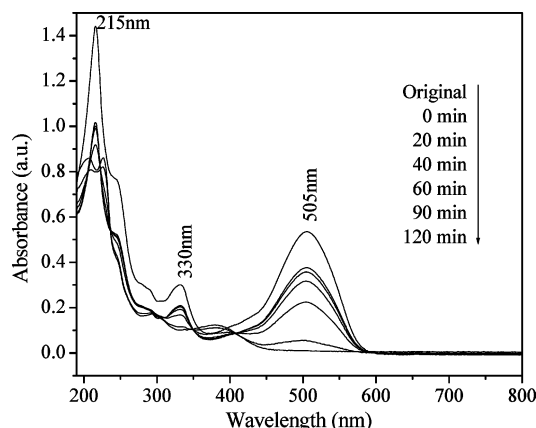


Figure 6. UV-vis spectral changes of ARG solution (50 mg/L) during the photocatalytic reaction by the $\text{Bi}_3\text{Nb}_{0.6}\text{Ta}_{0.4}\text{O}_7$ sample under visible light illumination.

cm^{-1} is attributed to the vibrations associated with uncoordinated NO_3^- ions, which are always exist in the raw material, indicating the presence of a trace amount of adsorbed NO_3^- in the as-synthesized product.⁴⁶ As shown in Figure 6, there are no significant differences between the two spectra and no characteristic peaks of ARG dye in the spectrum of the recovered $\text{Bi}_3\text{Nb}_{0.6}\text{Ta}_{0.4}\text{O}_7$ catalyst. The FT-IR analysis results confirm that the degradation of ARG dye is ascribed to the photocatalysis rather than physical adsorption and that the as-prepared catalyst is stable before and after the degradation.

Microcystin-LR (MC-LR) has been regarded as the most common and the most toxic variant among ~ 80 microcystins, and a provisional guideline value of 1 $\mu\text{g}/\text{L}$ for MC-LR in

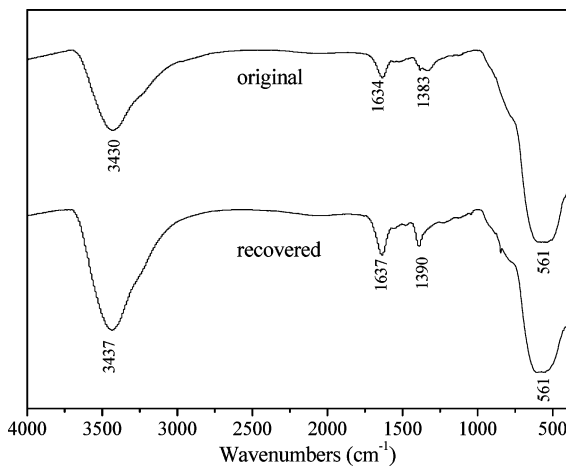


Figure 7. FT-IR spectra of the $\text{Bi}_3\text{Nb}_{0.6}\text{Ta}_{0.4}\text{O}_7$ catalyst before and after the photocatalytic reaction.

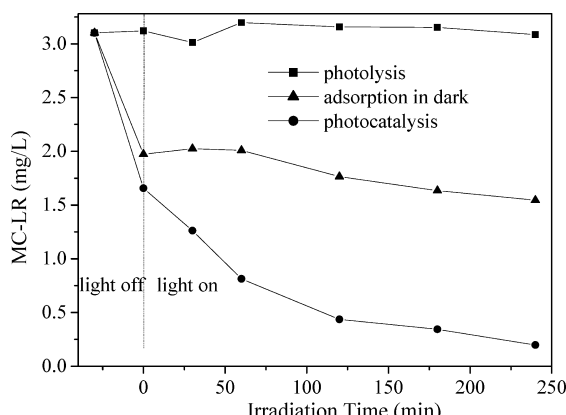


Figure 8. Photocatalytic degradation of MC-LR solution (3.1 mg/L) at pH = 5.9 over the $\text{Bi}_3\text{Nb}_{0.6}\text{Ta}_{0.4}\text{O}_7$ sample.

drinking water has been issued by the World Health Organization.⁴⁷ To further reveal the photocatalytic properties of the as-prepared $\text{Bi}_3\text{Nb}_x\text{Ta}_{1-x}\text{O}_7$ catalysts, MC-LR was selected to evaluate the photocatalytic activity. Figure 8 shows the decrease of the MC-LR concentration under visible light in the presence of the typical sample $\text{Bi}_3\text{Nb}_{0.6}\text{Ta}_{0.4}\text{O}_7$. As shown in Figure 8, no photolysis of MC-LR under visible light in the absence of catalyst is observed. The adsorption of MC-LR on the $\text{Bi}_3\text{Nb}_{0.6}\text{Ta}_{0.4}\text{O}_7$ sample in the dark was also checked. After 240 min, the concentration of MC-LR was decreased 49%. This result suggests that $\text{Bi}_3\text{Nb}_{0.6}\text{Ta}_{0.4}\text{O}_7$ has high adsorption ability for MC-LR, which is in favor of the photocatalytic reaction. However, with $\text{Bi}_3\text{Nb}_{0.6}\text{Ta}_{0.4}\text{O}_7$ as the photocatalyst, 94% of MC-LR was removed after visible light irradiation for 240 min, suggesting the $\text{Bi}_3\text{Nb}_{0.6}\text{Ta}_{0.4}\text{O}_7$ photocatalyst exhibits a high photocatalytic activity for degradation of MC-LR under visible light irradiation.

In this work, all the $\text{Bi}_3\text{Nb}_x\text{Ta}_{1-x}\text{O}_7$ solid solutions were observed to share a similar phase structure. The superiority photocatalytic activity of the $\text{Bi}_3\text{Nb}_x\text{Ta}_{1-x}\text{O}_7$ samples was mainly attributed to their narrow band gaps, small particle size, and the oxygen vacancies on the surface of the catalysts. A small band gap is effective in generating charge carriers. For the catalysts, the hybridization of O 2p and Bi 6s would push up the position of the valence band, resulting in the narrow band gaps.²³ Additionally, for nanoparticles, the diffusion length of electrons and holes (e^-/h^+) from the bulk to the surface is short, which helps to accelerate the migration rate of e^-/h^+ to the

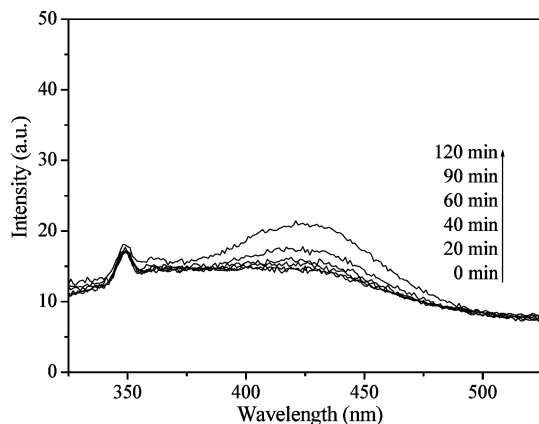


Figure 9. $\cdot\text{OH}$ trapping PL spectra of $\text{Bi}_3\text{Nb}_{0.6}\text{Ta}_{0.4}\text{O}_7$ on TA solution (0.5 g/L) under visible irradiation.

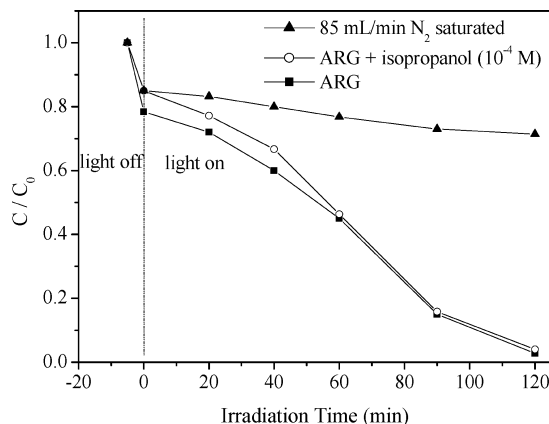
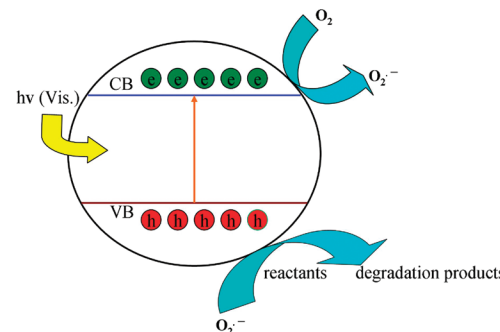


Figure 10. Photocatalytic degradation of ARG solution (50 mg/L) over $\text{Bi}_3\text{Nb}_{0.6}\text{Ta}_{0.4}\text{O}_7$ nanoparticles under different conditions.

surface of the nanoparticle to participate in the reaction process.⁴⁸ Furthermore, the compounds Bi_3NbO_7 and Bi_3TaO_7 both crystallize in a defect fluorite-type structure with distorted octahedral coordination geometry and exhibit intrinsic oxygen vacancies and a disorder in both anionic and cationic lattices.³⁶ Therefore, during the process of photocatalytic reactions, the oxygen vacancies in the structure of compounds $\text{Bi}_3\text{Nb}_x\text{Ta}_{1-x}\text{O}_7$, which are isostructural with Bi_3NbO_7 , may become the centers to capture photoinduced electrons so that the recombination of photoinduced electrons and holes could be effectively inhibited, resulting in the higher quantum efficiency of photocatalysis.^{49,50} The distorted octahedral coordination geometry in the structure can also improve the mobility of photogenerated charge carriers and enhances its visible light photocatalytic properties.^{38,51}

For the photocatalytic process, photoinduced electrons or holes emerging over a semiconductor directly or indirectly react with O_2 and OH^- to form $\text{O}_2^{\bullet-}$ and $\cdot\text{OH}$ oxidative species.⁵² As shown in Figure 9, the fluorescence intensity at 426 nm is very low, which elucidates that $\cdot\text{OH}$ on $\text{Bi}_3\text{Nb}_{0.6}\text{Ta}_{0.4}\text{O}_7$ catalyst is hardly produced under visible light irradiation. In another experiment, it was found that the addition of isopropanol, a well-known scavenger of $\cdot\text{OH}$ radicals,⁵³ into the photoreaction system did not cause the apparent changes in the degradation rate of ARG, as shown in Figure 10. The results indicate that the free $\cdot\text{OH}$ radicals could not be the main active oxygen species in this photochemical process, which is different from TiO_2 toward photocatalytic degradation of organic pollutants.^{54,55} As mentioned above, the sample shows the excellent photocatalytic activity under visible light irradiation. Therefore, it could be postulated that $\text{O}_2^{\bullet-}$ is the other pivotal active species

SCHEME 1: Proposed Mechanism for the Photocatalytic Degradation of Organic Pollutants over $\text{Bi}_3\text{Nb}_x\text{Ta}_{1-x}\text{O}_7$ Photocatalysts



for $\text{Bi}_3\text{Nb}_{0.6}\text{Ta}_{0.4}\text{O}_7$ photocatalysis. The $\text{O}_2^{\bullet-}$ could be formed by photogenerated electron reacting directly with O_2 adsorbed on the surface of the catalyst. The photocatalytic reactivity with continuous N_2 sparging and thus in a stricter anoxic condition was checked. As can be seen in Figure 10, the photodegradation rate of ARG was largely prohibited under the anoxic suspension. Apparently, the presence of oxygen is responsible for the significant reduction. The presence of oxygen is to primarily act as an efficient e^- trap, leading to the generation of $\text{O}_2^{\bullet-}$ and preventing the recombination of e^- and h^+ .⁵³ On the basis of the discussion above, a possible mechanism for the photodegradation of organic pollutants has been proposed (Scheme 1).

4. Conclusions

In summary, efficient visible-light-induced $\text{Bi}_3\text{Nb}_x\text{Ta}_{1-x}\text{O}_7$ nanoparticles were synthesized by a facile and low-cost sol-gel method using stable, less toxic Ta_2O_5 , Nb_2O_5 , and $\text{Bi}(\text{NO}_3)_3 \cdot 5\text{H}_2\text{O}$ as the raw materials. The optical band gaps of the $\text{Bi}_3\text{Nb}_x\text{Ta}_{1-x}\text{O}_7$ nanoparticles were estimated to be about 2.80 eV. The average crystal size of the as-prepared samples was only about 15 nm. These photocatalysts exhibited strong photocatalytic activity for the degradation of ARG under visible light irradiation. Moreover, the typical sample $\text{Bi}_3\text{Nb}_{0.6}\text{Ta}_{0.4}\text{O}_7$ also showed excellent photocatalytic properties for the removal of MC-LR. Kinetic studies by using $\cdot\text{OH}$ trapping PL spectra and the radical scavenger technologies suggest that $\cdot\text{OH}$ is not the dominant photooxidant. The $\text{O}_2^{\bullet-}$ is the pivotal active species for $\text{Bi}_3\text{Nb}_x\text{Ta}_{1-x}\text{O}_7$ photocatalysis. These results suggested that $\text{Bi}_3\text{Nb}_x\text{Ta}_{1-x}\text{O}_7$ is the prominent materials for photooxidation of organics in the range of visible light.

Acknowledgment. This work was supported by the National Natural Science Foundation of China (50872013), National Basic Research Program of China (973 Program) 2007CB613302, and the Key Project of Chinese Ministry of Education (No. 108164).

References and Notes

- Fox, M. A.; Dulay, M. T. *Chem. Rev.* **1993**, *93*, 341.
- Yu, J. C.; Yu, J. G.; Ho, W. K.; Jiang, Z. T.; Zhang, L. Z. *Chem. Mater.* **2002**, *14*, 3808.
- Kapoor, M. P.; Inagaki, S.; Yoshida, H. *J. Phys. Chem. B* **2005**, *109*, 9231.
- Kaneko, M.; Gokan, N.; Kataoka, N.; Takei, Y.; Hoshino, M. *Chem. Commun.* **2005**, *12*, 1625.
- Martin, S. T.; Lee, A. T.; Hoffmann, M. R. *Environ. Sci. Technol.* **1995**, *29*, 2567.
- Adachi, M.; Murata, Y.; Takao, J.; Jiu, J. T.; Sakamoto, M.; Wang, F. M. *J. Am. Chem. Soc.* **2004**, *126*, 14943.
- Yu, J. C.; Zhang, L. Z.; Yu, J. G. *Chem. Mater.* **2002**, *14*, 4647.

- (8) Kawahara, T.; Konishi, Y.; Tada, H.; Tohge, N.; Nishii, J.; Ito, S. *Angew. Chem., Int. Ed.* **2002**, *41*, 2811.
- (9) Choi, W.; Termin, A.; Hoffmann, M. R. *J. Phys. Chem.* **1994**, *98*, 13669.
- (10) Zhou, J. K.; Lv, L.; Yu, J. Q.; Li, H. L.; Guo, P. Z.; Sun, H.; Zhao, X. S. *J. Phys. Chem. C* **2008**, *112*, 5316.
- (11) Zhang, G. K.; Ding, X. M.; Hu, Y. J.; Huang, B. B.; Zhang, X. Y.; Qin, X. Y.; Zhou, J.; Xie, J. W. *J. Phys. Chem. C* **2008**, *112*, 17994.
- (12) Sakthivel, S.; Kisch, H. *Angew. Chem., Int. Ed.* **2003**, *42*, 4908.
- (13) Zhao, W.; Ma, W. H.; Chen, C. C.; Zhao, J. C.; Shuai, Z. G. *J. Am. Chem. Soc.* **2004**, *126*, 4782.
- (14) Anpo, M. *Catal. Surv. Jpn.* **1997**, *1*, 169.
- (15) Kudo, A.; Omori, K.; Kato, H. *J. Am. Chem. Soc.* **1999**, *121*, 11459.
- (16) Sun, S. M.; Wang, W. Z.; Zhang, L.; Zhou, L.; Yin, W. Z.; Shang, M. *Environ. Sci. Technol.* **2009**, *43*, 2005.
- (17) Ishikawa, A.; Takata, T.; Matsumura, T.; Kondo, J. N.; Hara, M.; Kobayashi, H.; Domen, K. *J. Phys. Chem. B* **2004**, *108*, 2637.
- (18) Kako, T.; Zou, Z. G.; Katagiri, M.; Ye, J. H. *Chem. Mater.* **2007**, *19*, 198.
- (19) Maeda, K.; Hashiguchi, H.; Masuda, H.; Abe, R.; Domen, K. *J. Phys. Chem. C* **2008**, *112*, 3447.
- (20) Wei, W.; Dai, Y.; Huang, B. B. *J. Phys. Chem. C* **2009**, *113*, 5658.
- (21) Zhang, X.; Zhang, L. Z.; Xie, T. F.; Wang, D. J. *J. Phys. Chem. C* **2009**, *113*, 7371.
- (22) Zhang, G. K.; Yang, J. L.; Zhang, S. M.; Xiong, Q.; Huang, B. B.; Wang, J. T.; Gong, W. Q. *J. Hazard. Mater.* (DOI: 10.1016/j.jhazmat.2009.07.089).
- (23) Kim, H. G.; Hwang, D. W.; Lee, J. S. *J. Am. Chem. Soc.* **2004**, *126*, 8912.
- (24) Yoshino, M.; Kakihana, M.; Cho, W. S.; Kato, H.; Kudo, A. *Chem. Mater.* **2002**, *14*, 3369.
- (25) Ebina, Y.; Tanaka, A.; Kondo, J. N.; Domen, K. *Chem. Mater.* **1996**, *8*, 2534.
- (26) Zhang, G. K.; Zou, X.; Gong, J.; He, F. S.; Zhang, H.; Zhang, Q.; Liu, Y.; Yang, X.; Hu, B. *J. Alloys Compd.* **2006**, *425*, 76.
- (27) Nyman, M.; Rodriguez, M. A.; Rohwer, L. E. S.; Martin, J. E.; Waller, M.; Osterloh, F. E. *Chem. Mater.* (DOI: 10.1021/cm9020645).
- (28) Liu, M. N.; Xue, D. F. *Mater. Lett.* **2005**, *59*, 2908.
- (29) Niederberger, M.; Pinna, N.; Polleux, J.; Antonietti, M. *Angew. Chem., Int. Ed.* **2004**, *43*, 2270.
- (30) Liu, M. N.; Xue, D. F.; Luo, C. *J. Am. Ceram. Soc.* **2006**, *89*, 1551.
- (31) Zhang, G. K.; Hu, Y. J.; Ding, X. M.; Zhou, J.; Xie, J. W. *J. Solid State Chem.* **2008**, *181*, 2133.
- (32) Hirakawa, T.; Nosaka, Y. *Langmuir* **2002**, *18*, 3247.
- (33) Wu, J.; Duan, F.; Zheng, Y.; Xie, Y. *J. Phys. Chem. C* **2007**, *111*, 12866.
- (34) Dunkle, S. S.; Suslick, K. S. *J. Phys. Chem. C* **2009**, *113*, 10341.
- (35) Castro, A.; Aguado, E.; Rojo, J. M.; Herrero, P.; Enjalbert, R.; Galy, J. *Mater. Res. Bull.* **1998**, *33*, 31.
- (36) Abrahams, I.; Krok, F.; Struzik, M.; Dygas, J. R. *Solid State Ionics* **2008**, *179*, 1013.
- (37) Jovalekic, C.; Pavlovic, M.; Osmokrovic, P.; Atanasoska, L. *Appl. Phys. Lett.* **1998**, *72*, 1051.
- (38) Zhang, G. K.; Zou, X.; Gong, J.; He, F. S.; Zhang, H.; Ouyang, S. X.; Liu, H. X.; Zhang, Q.; Liu, Y.; Yang, X.; Hu, B. *J. Mol. Catal. A: Chem.* **2006**, *255*, 109.
- (39) Atanassova, E.; Spassov, D.; Paskaleva, A.; Kostov, K. *Appl. Surf. Sci.* **2006**, *253*, 2841.
- (40) Butler, M. A. *J. Appl. Phys.* **1977**, *48*, 1914.
- (41) Tang, J.; Zou, Z.; Ye, J. *J. Phys. Chem. B* **2003**, *107*, 14265.
- (42) Zhou, D.; Wang, H.; Yao, X.; Pang, L. X. *Mater. Chem. Phys.* **2008**, *110*, 212.
- (43) Dharmaraj, N.; Park, H. C.; Kim, C. H.; Viswanathamurthi, P.; Kim, H. Y. *Mater. Res. Bull.* **2006**, *41*, 612.
- (44) Kavanagh, Y.; Alam, M. J.; Cameron, D. C. *Thin Solid Films* **2004**, *85*, 447.
- (45) Compton, O. C.; Osterloh, F. E. *J. Phys. Chem. C* **2009**, *113*, 479.
- (46) Zhang, Y. W.; Si, R.; Liao, C. S.; Yan, C. H.; Xiao, C. X.; Kou, Y. *J. Phys. Chem. B* **2003**, *107*, 10159.
- (47) Nybom, S. M. K.; Carmen Collado, M.; Surono, I. S.; Salminen, S. J.; Meriluoto, J. A. O. *J. Agric. Food Chem.* **2008**, *56*, 3714.
- (48) Hagfeldt, A.; Grätzel, M. *Chem. Rev.* **1995**, *95*, 49.
- (49) Xiao, Q.; Zhang, J.; Xiao, C.; Tan, X. K. *Mater. Sci. Eng., B* **2007**, *142*, 121.
- (50) Wang, Y. X.; Li, X. Y.; Wang, N.; Quan, X.; Chen, Y. Y. *Sep. Purif. Technol.* **2008**, *62*, 727.
- (51) Ziolek, M. *Catal. Today* **2003**, *78*, 47.
- (52) Lin, X. P.; Huang, F. Q.; Wang, W. D.; Shan, Z. C.; Shi, J. L. *Dyes Pigm.* **2008**, *78*, 39.
- (53) Fu, H. B.; Pan, C. S.; Yao, W. Q.; Zhu, Y. F. *J. Phys. Chem. B* **2005**, *109*, 22432.
- (54) Wold, A. *Chem. Mater.* **1993**, *5*, 280.
- (55) Chiou, C. H.; Wu, C. Y.; Juang, R. S. *Sep. Purif. Technol.* **2008**, *62*, 559.

JP907831Y